Accessibility and Ion Exchange Stoichiometry of Ionized Carboxylic Groups in the Active Layer of FT30 Reverse Osmosis Membrane

ARTICLE *in* ENVIRONMENTAL SCIENCE AND TECHNOLOGY · AUGUST 2009

Impact Factor: 5.33 · DOI: 10.1021/es803595f · Source: PubMed

3 AUTHORS, INCLUDING:

David G Cahill
University of Illinois, Urbana-Champaign
365 PUBLICATIONS **13,998** CITATIONS

Environ. Sci. Technol. **2009,** *43,* 5042–5048

Accessibility and Ion Exchange Stoichiometry of Ionized Carboxylic Groups in the Active Layer of FT30 Reverse Osmosis Membrane

ORLANDO CORONELL,[†,§] BENITO J. MARIÑAS,[*,†,§] AND DAVID G. CAHILL[‡,§]

Department of Civil and Environmental Engineering, Department of Materials Science and Engineering, and Science and Technology Center of Advanced Materials for the Purification of Water with Systems, University of Illinois at Urbana−Champaign, Urbana, Illinois 61801

Received December 26, 2008. Revised manuscript received April 26, 2009. Accepted April 28, 2009.

We have experimentally determined the concentration of Ba^{2+} that associates with the accessible ionized R—COO^- groups in the polyamide active layer of the FT30 reverse osmosis membrane in the pH range 3.42−10.30. Ba^{2+} concentrations in the active layer ($[Ba^{2+}]$) were measured using the ion-probing/Rutherford backscattering spectrometry procedure reported in our previous work. We found that at all but the lowest experimental pH 3.42, $[Ba^{2+}]$ was lower than the corresponding total concentrations of R—COO^- groups; their difference was consistent with steric and charge effects determining the accessibility and association, respectively, of Ba^{2+} to R—COO^- groups. Accordingly, we propose two descriptors, the *accessibility ratio* (AR) and the *neutralization number* (NN), to account for the observed difference. AR, the fraction of R—COO^- groups accessible to Ba^{2+} ions, and NN, the average number of R—COO^- groups neutralized per Ba^{2+} ion, were determined experimentally performing Ag^+-Ba^{2+} ion-exchange tests. The resulting AR = 0.40 indicated that on average only 40% of ionizable carboxylic groups were accessible to Ba^{2+}. $[Ba^{2+}]$ values calculated using R—COO^- concentrations and the AR and NN concepts were in agreement with experimental $[Ba^{2+}]$ results.

Introduction

Most commercially available reverse osmosis (RO) and nanofiltration (NF) membranes have a thin-film composite structure consisting of a top thin polyamide active layer (∼50−200 nm), an intermediate polysulfone support (∼50 μm) and a backing (∼200 μm) of nonwoven polyester fibers (*1*). Some membranes also have a protective surface coating designed to produce a more hydrophilic, fouling-resistant surface (*1, 2*). The active layer of RO/NF membranes is the main barrier controlling contaminant rejection which is the result of solute-active layer interactions determining the ability of contaminants to partition into and move through the active layer (*1, 3*), with active layer pore size and charge distribution, and contaminant size and charge playing important roles in transport phenomena (*3*−*5*). Accordingly, comparing how solutes with different sizes and charges interact with active layers would improve our understanding of the mechanisms controlling contaminant transport through RO/NF membranes.

Unfortunately, characterizing contaminant-active layer interactions has remained challenging due to limitations associated with the nanometer-scale spatial resolution required to study these ultrathin active layers. Several groups have addressed this challenge by characterizing the physicochemical properties of active layers and the concentration of contaminants within them through different thin-film characterization procedures (*6*–*13*). In one of these procedures of interest for the present study, we quantified the concentrations of ionized functional groups in the polyamide active layer of the FT30 reverse osmosis (RO) membrane as a function of pH (*14*). While ionized carboxylic groups (R—COO^-) were above detection limit (∼0.01 M) in the pH range studied (∼3.5−10.3), ionized amine groups (R—NH_3^+) decreased below detection limit above pH 6.0. Total concentrations of carboxylic (≈0.43 M) and amine (≈0.04 M) groups were in the same order of magnitude of theoretical predictions by Freger and Srebnik (*15*), and of experimental volumetric charge densities and ion exchange capacities obtained from streaming potential analysis and titration methods, respectively, for various polyamide active layers (*4, 16*).

The procedure for quantification of R—COO^- groups involved their neutralization with Ag^+ as ion probe followed by the quantification of Ag^+ by Rutherford backscattering spectrometry (RBS). Ag^+ was chosen as probe because it fulfilled two requirements: (i) smaller ionic radius (r_{Ag^+} = 0.81−1.42 Å (*17*)) than the radii of the smallest pores in the active layer of FT30 membrane ($r_{Pore\ min}$ = 1.4−2.3 Å (*8*)); and (ii) accurate quantification by RBS (*18*) at the concentrations that R—COO^- is present in polyamide active layers (i.e., RBS signal is proportional to the square of the atomic number of the element detected). The size of the smallest pores in the active layer of the FT30 membrane was previously determined by Kim et al. (*8*) in a positron annihilation lifetime spectroscopy (PALS) study that found a bimodal pore size distribution with larger and smaller pore radii in the ranges of 3.5−4.1 Å and 1.4−2.3 Å, respectively. The results from Kim et al. are consistent with later results of similar PALS studies for different RO/NF membranes (*9*).

The concentration of Ag^+ in the active layer ($[Ag^+]$) measured by RBS was assumed to be equivalent to that of R—COO^- groups based on two premises (*14*): (i) accessibility of Ag^+ to all R—COO^- groups due to $r_{Ag^+} \leq r_{Pore\ min}$ (see Figure 1); and (ii) one-to-one correspondence between Ag^+ ions and R—COO^- groups due to the monovalence of both. It was also implicitly assumed that $[Ag^+]$ was not significantly affected by formation of Ag^+−amine complexes; this assumption was supported by a 10-fold difference between the calculated total concentrations of carboxylic (≈0.43 M) and amine (≈0.04 M) groups in FT30 membrane (*14, 15*). Additionally, the stability constants for Ag^+−amine complexes in aqueous solutions (*19*) indicate that no more than ∼75% and ∼1% of R—NH_2 would complex with Ag^+ to form $(amine)_2Ag^+$ and $(amine)Ag^+$ complexes, respectively. As amine groups are in relatively low concentrations and relatively fixed positions in the polymer matrix, it seems unlikely that $(amine)_2Ag^+$ complexes form; however, in a worst case scenario, each Ag^+ would complex with two

* Corresponding author phone: +1-217-333-6961; fax: +1-217-333-6968; e-mail: marinas@uiuc.edu.
† Department of Civil and Environmental Engineering.
‡ Department of Materials Science and Engineering.
§ Science and Technology Center of Advanced Materials for the Purification of Water with Systems.

10.1021/es803595f CCC: $40.75

Published on Web 05/27/2009

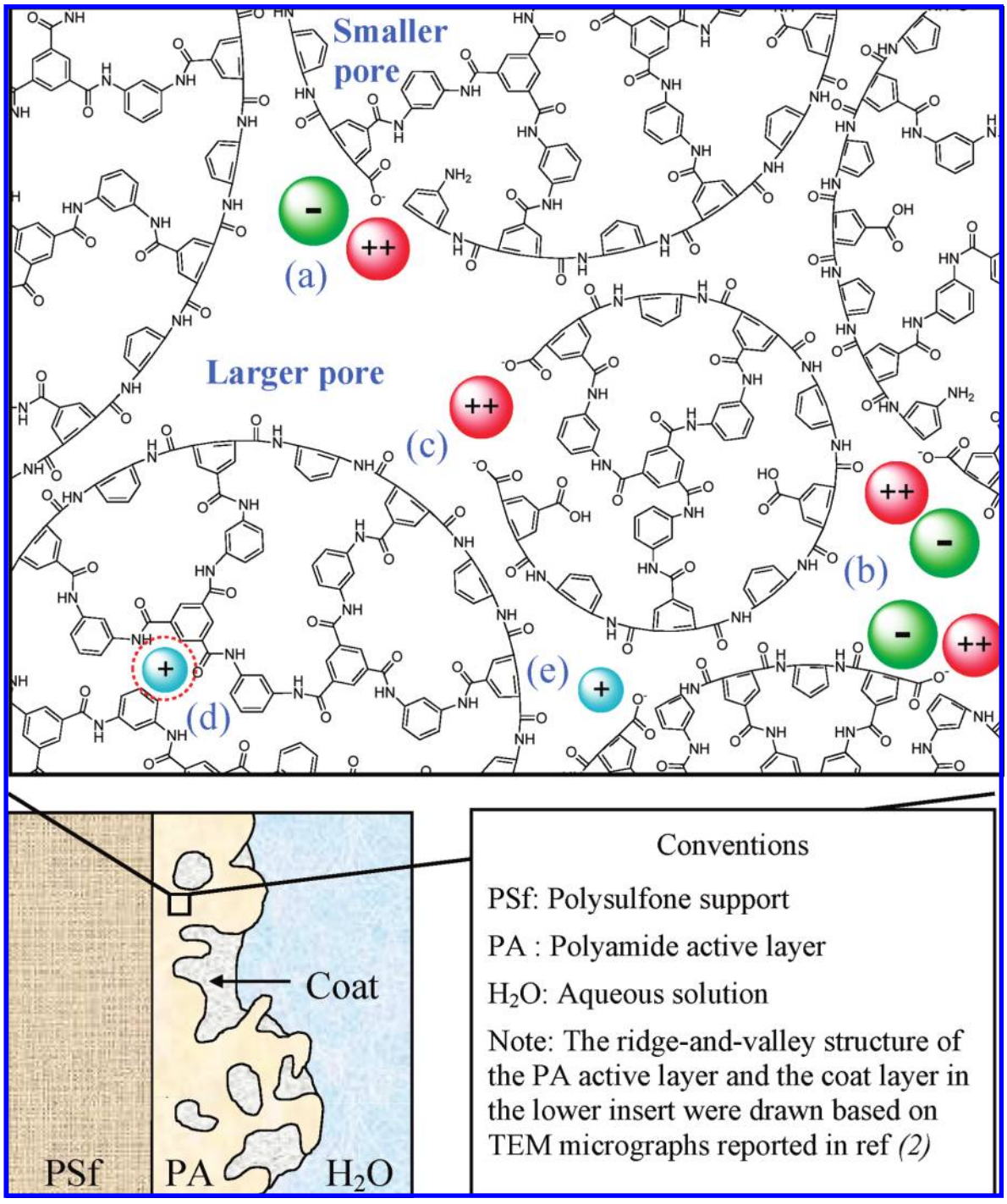

FIGURE 1. Top: Schematic representation of the accessibility and association of counterions to ionized carboxylic groups (R—COO⁻) in the bulk polyamide active layer of the FT30 RO membrane. The figure is not intended as an exact representation of the molecular structure of the polyamide network, but as a visual aid to the accessibility and stoichiometry of association concepts discussed in this manuscript. Larger and smaller pores represent the bimodal pore size distribution reported by Kim et al. (*8*). Monovalent (blue) positive and (green) negative circles represent silver and chloride ions, respectively. Divalent (red) circles represent barium ions. Bottom: Composite structure of the FT30 RO membrane showing the open ridge-and-valley structure of its polyamide active layer where steric effects may be negligible for counterions accessing ionized functional groups located in the vicinity of the surface. The cartoon also shows the coat layer on top of the active layer which was previously reported (*14*) to have a composition consistent with that of 50% ester-cross-linked polyvinyl alcohol.

$R—NH_2$ groups, and therefore the uncertainty in the concentration of $R—COO^-$ groups measured with our ion-probe method should not exceed $(0.04\ M \times 0.75) \div 2 = 0.015\ M$.

The ion-probing/RBS procedure previously developed to quantify the concentration of $R—COO^-$ groups in the active layer of FT30 membrane (*14*) opens the possibility to study the accessibility and ion-exchange stoichiometry of $R—COO^-$ groups by using ion probes of varying size and charge. Accordingly, the objectives of this study are to quantify as a function of pH in the active layer of the FT30 membrane: (i) the accessibility of Ba^{2+} ion ($r_{Ba^{2+}} = 1.49-1.75$ Å (*17*)) to $R—COO^-$ groups; and (ii) the ion-exchange stoichiometry between (divalent) Ba^{2+} ion and $R—COO^-$ groups. To accomplish these objectives, we measured the concentra-

tion of Ba^{2+} that associates as a function of pH with the accessible R—COO^- groups in the active layer of the FT30 membrane, and compared the results to those previously obtained with the relatively smaller and monovalent Ag^+. The results from this study constitute the first direct quantification of the steric effects and stoichiometry of association of ionic contaminants within the active layers of RO/NF membranes. We also developed a conceptual and mathematical model describing the results.

Materials and Methods

(See extended version in the Supporting Information)

Target Membrane. All experiments were performed with coupons (2.5 × 5.0 cm^2) of the thin-film composite FT30 RO membrane (Dow Liquid Separation, Midland, MI) cut from a spiral-wound element.

Ion-Probe Solutions. All chemicals used were ACS grade with 99%+ purity. Silver nitrate ($AgNO_3$), barium nitrate ($Ba(NO_3)_2$), and barium chloride dihydrate ($BaCl_2 \cdot 2H_2O$) were used as sources of Ag^+ and Ba^{2+}. All ion-probe solutions were prepared with nanopure water. The concentrations of silver (5×10^{-5}–10^{-3} M) and barium (10^{-6}–0.32 M) in solution were always below their solubility limit at the pH tested. The pH of barium and silver solutions was adjusted to the desired value by addition of HCl or NaOH, and HNO_3 or NaOH, respectively.

Sample Preparation for Ion Probing with Ba^{2+}. Membrane coupons previously rinsed with nanopure water were immersed in 0.1 M $BaCl_2 \cdot 2H_2O$ solution at the pH of interest to saturate accessible R—COO^- groups with Ba^{2+}. Then, to reduce excess Ba^{2+} not associated to R—COO^- groups to a concentration below the detection limit of our sample analysis procedure, the samples underwent four immersions in 10^{-6} M $BaCl_2 \cdot 2H_2O$ solution at the same pH used in the saturation step. Finally, the samples were dried by pressing them between two filter-papers and air-dried at room temperature for ≥ 24 h. Each experimental pH condition was tested in triplicate. All membrane coupons used for Ba^{2+}-probing tests were cut from approximately the same location (FT30-L1) of the spiral-wound element.

Sample Preparation for Ag^+/Ba^{2+} Ion Exchange. Ion-exchange experiments in the pH range 7.5–10.3 were performed to study the displacement of Ag^+ by Ba^{2+} from the R—COO^- groups in the active layer of FT30 membrane. Sample preparation was similar to that for Ba^{2+}-probing tests with some modifications. After rinsing with nanopure water, the coupons were immersed in concentrated $AgNO_3$ solution at the target pH to saturate R—COO^- groups with Ag^+. Next, exchange of Ag^+ by Ba^{2+} was effected by sequential immersions in 0.32 and 0.10 M $Ba(NO_3)_2$ solutions at the same target pH used in the Ag^+-saturation step. Then, to reduce excess ions not associated to R—COO^- groups to a concentration several orders of magnitude below the detection limit of our sample analysis procedure, the samples underwent four immersions in 10^{-6} M $Ba(NO_3)_2$ solution at the same target pH of the previous steps. Coupons used as test samples were cut from four different locations (FT30-L2 through FT30-L5) of the spiral-wound element. Experiments were performed in triplicate at pH values of ~7.5 (FT30-L4 and FT30-L5), ~9.5 (FT30-L2 and FT30-L3), and ~10.3 (FT30-L5).

Sample Analysis. RBS was used to quantify Ba^{2+} and Ag^+ concentrations in the active layer of treated membrane samples. Extensive information on RBS theory and analysis (*18, 20*), and use in polymer and membrane characterization (*6, 11, 21*) can be found elsewhere. In this study, immediately before sample analysis, the membrane coupons were attached to the sample holder of the RBS analysis chamber at room temperature using a double-sided thermally conductive adhesive tape. Next, a circular, 3 mm, 2-MeV He^+ beam generated with a Van de Graaff accelerator was scanned over the surface of the membrane sample. Incident, exit, and scattering angles of the He^+ beam were 22.5°, 52.5°, and 150°, respectively. A detector registered the energy and counts of backscattered ions (see sample spectrum in Supporting Information (SI) Figure S2). For a given incident ion, geometry of RBS setup, and energy of the incident beam, the energy of the backscattered ions reveals the elements present in the sample; the counts at each energy serve to obtain the relative concentrations of each element without the need of calibration standards (*18, 20*). Only hydrogen cannot be detected directly by RBS, and so a theoretical hydrogen/carbon ratio of 0.67 was assumed (*11*). The software SIMNRA (*18*) was used for data analysis. For details on the calculation of ion-probe concentrations in the active layer, please see extended version of the Sample Analysis section in the SI. Also, the carboxylic group concentrations in the active layer of the FT30 membrane presented in this study in Figure 2a were obtained using $\rho_{active\ layer} = 1.24$ g/cm^3 (*22*) to improve the accuracy of the corresponding concentrations previously reported (*14*) where $\rho_{active\ layer} = 1.06$ g/cm^3 was assumed. The newly calculated values are ~11% higher

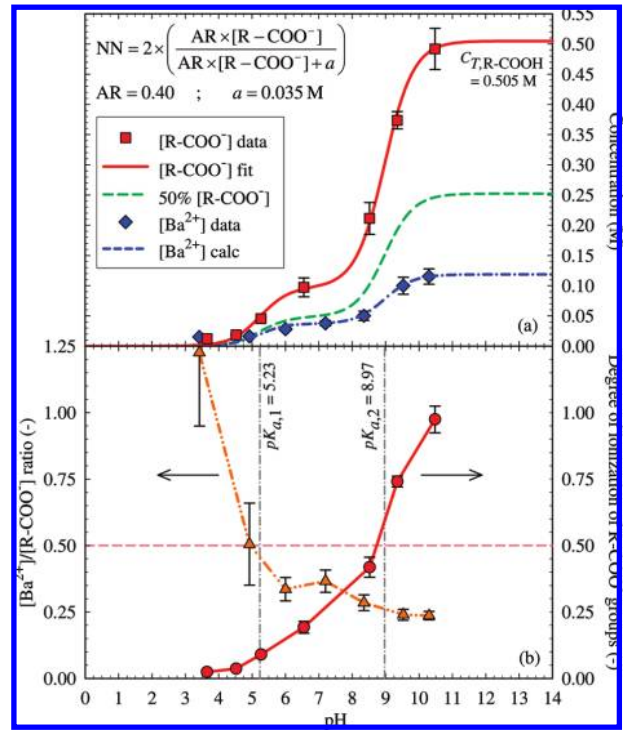

FIGURE 2. (a) Comparison between the total concentration of R—COO^- groups ([R—COO^-]) in the polyamide active layer of the FT30 RO membrane as a function of pH and the concentration of barium ions that ionically associate with accessible R—COO^- groups ([Ba^{2+}]). Error bars indicate standard deviation. The [R—COO^-] data points (red symbols), and corresponding model fit (continuous red curve) for the acid–base equilibrium between R—COO^- groups and the aqueous solution, were obtained by using $\rho_{active\ layer}$ = 1.24 g/cm^3 (*22*) to improve the accuracy of the [R—COO^-] values previously calculated in ref *14* where $\rho_{active\ layer}$ = 1.06 g/cm^3 was assumed (see extended version of the Sample Analysis section in the SI for details). The (blue) dashed-dotted line corresponds to the calculated [Ba^{2+}] as a function of pH using eq 2. (b) [Ba^{2+}]/[R—COO^-] ratio as a function of pH (orange triangles) and degree of ionization of R—COO^- groups (red circles). The (orange) dash-dot-dot and (red) continuous lines correspond to straight lines connecting the experimental data points. Error bars indicate standard error. The horizontal (pink) dashed line represents the minimum possible [Ba^{2+}]/[R—COO^-] ratio of 0.5 if 100% of the R—COO^- groups were accessible to Ba^{2+} ions.

than those reported in (*14*). See also extended version of the Sample Analysis in the SI for details.

Results and Discussion

Concentration of Ba^{2+} Ion Associated with R—COO^- Groups ([Ba^{2+}]). Figure 2a shows a comparison between the concentration of R—COO^- groups ([R—COO^-]) in the polyamide active layer of FT30 RO membrane as a function of pH and the concentration of Ba^{2+} that associates with them ([Ba^{2+}]). Experimental [R—COO^-] concentrations (red squares) and corresponding fit line (continuous red curve) from our modeling results based on acid−base equilibrium between R—COO^- groups and aqueous solution correspond to the values reported in our previous work (*14*) corrected using $\rho_{\text{active layer}} = 1.24$ g/cm^3 as detailed above. [Ba^{2+}] (blue diamonds) was measured as part of the present study through ion-probing/RBS analysis. The figure shows that [Ba^{2+}] was consistently lower than [R—COO^-] and the (green) dashed line representing 50% of the concentration of R—COO^- groups. Consequently, the [Ba^{2+}] results could not be explained based solely on the assumption that, because of their divalence, each Ba^{2+} ion neutralizes two R—COO^- groups simultaneously.

To evaluate the possible causes for the difference between [R—COO^-] and [Ba^{2+}], we used the information from Figure 2a to calculate the [Ba^{2+}]/[R—COO^-] ratio (orange triangles) as a function of pH, and plotted it in Figure 2b together with the degree of ionization of carboxylic groups, i.e., [R—COO^-]/([R—COOH]+[R—COO^-]) (red circles). The two vertical dashed-dotted lines correspond to the two pK_a values that describe the ionization behavior of carboxylic groups in the active layer of FT30 membrane (*14*). Figure 2b shows that at the lowest experimental pH 3.42, the [Ba^{2+}]/[R—COO^-] ratio was not significantly different from one, which suggests that all R—COO^- groups were accessible to Ba^{2+}, and that there was a one-to-one correspondence between *monovalent* R—COO^- groups and *divalent* Ba^{2+} ions (see locations (a) and (b) in Figure 1). Such one-to-one correspondence is consistent with the relatively low concentration (≈0.01 M) of R—COO^- groups at pH 3.42. Assuming a homogeneous distribution of R—COO^- groups throughout the polyamide matrix, the average distance between neighboring ionized sites would be ≈5.5 nm making it relatively unlikely for one Ba^{2+} ion to neutralize two R—COO^- groups. We also estimated the average separation between R—COO^- groups at a concentration of 0.50 M (i.e., the total concentration of ionizable carboxylic groups in FT30 membrane). Under the same assumption of R—COO^- groups homogeneously distributed, the average distance between neighboring ionized sites would decrease to ≈1.5 nm, therefore increasing the probability of the existence of Ba^{2+} ions neutralizing two R—COO^- sites simultaneously (see location (c) in Figure 1).

Consistent with the discussion above, we expect the *average* distance between neighboring ionized sites in FT30 membrane to decrease with increasing pH (i.e., with increasing concentration of R—COO^- groups), and the *average* number of R—COO^- groups neutralized per Ba^{2+} ion to *gradually* increase from one to two. Consequently, even though the difference between [R—COO^-] and [Ba^{2+}] in Figure 2a could not be explained based only on the divalence of Ba^{2+}, we propose that the divalence does play a role in the observed difference with a stronger effect as pH increases. Accordingly, defining the *neutralization number* (NN) for Ba^{2+} at a certain solution pH as the average number of R—COO^- groups neutralized per Ba^{2+} ion, and assuming that Ba^{2+} has access to 100% of the ionized sites in the active layer, then [Ba^{2+}] could be expressed by eq 1.

$$[Ba^{2+}] = \frac{[R{-}COO^-]}{NN} \qquad (1)$$

To evaluate the assumption of 100% accessibility of Ba^{2+} to R—COO^- groups, we drew a (pink) dashed line in Figure 2b corresponding to the theoretical minimum [Ba^{2+}]/[R—COO^-] = 0.5 ratio if Ba^{2+} had access to all R—COO^- groups; for 100% accessibility, all R—COO^- groups would be neutralized by Ba^{2+} and each Ba^{2+} ion would neutralize at most two ionized sites. Figure 2b shows that the experimental [Ba^{2+}]/[R—COO^-] ratio was lower than the theoretical minimum value of 0.5 at all but the two lowest experimental pH values, and that there was a rapid decrease of the [Ba^{2+}]/[R—COO^-] ratio from ≈1 to less than 0.5 in the pH range 3.42−6.00. Accordingly, the results suggest that the accessibility of Ba^{2+} to R—COO^- groups decreased in the initial ionization stages, and that only the carboxylic groups ionizable at the lowest experimental pH 3.42 were 100% accessible to Ba^{2+}. Figure 2b also shows that the R—COO^- groups ionized at pH 3.42 are only ≈2.5% of all ionizable carboxylic groups detected.

The general upper limits of the pK_a values of monobasic and polybasic carboxylic groups in bulk water at 25 °C are ≈5.0 and ≈6.4, respectively (*23*). As a result, the relatively low pH of ionization of the carboxylic groups deprotonated at pH 3.42 suggests that they are exposed to bulk aqueous solution, and that they might be located in the vicinity of the open ridge-and-valley structure (*1, 2*) at the surface of the polyamide active layer (see bottom-left schematic of Figure 1).

As mentioned above, Figure 2b shows that the [Ba^{2+}]/[R—COO^-] ratio was below 0.5 at pH ≥ 6. This indicates that in most of the pH range studied a fraction of the ionized R—COO^- groups was inaccessible to Ba^{2+} ($r_{Ba^{2+}} = 1.49-1.75$ Å (*17*)) but accessible to the smaller Ag^+ ($r_{Ag^+} = 0.81-1.42$ Å (*17*)). Such observation suggests that Ba^{2+} ions experience steric effects in the active layer (see location (d) in Figure 1) that prevent their access to a fraction of the R—COO^- groups (see location (e) in Figure 1). Since hindered accessibility was observed in most of the pH range studied, we conclude that most of the carboxylic groups in the active layer are located in the bulk of the polyamide matrix where steric effects are important for Ba^{2+} ion. Counterion exclusion by steric effects has also been reported to occur in ion-exchange resins and zeolites (*24*). As counterion size increases, ion-exchange materials may show an apparent reduction in ion-exchange capacity indicating the occurrence of steric effects that limit counterion accessibility to functional groups (*24*).

We used the concept of hindered accessibility of Ba^{2+} to carboxylic groups to modify eq 1 by defining the *accessibility ratio* (AR) for Ba^{2+} as the fraction of R—COO^- groups accessible to Ba^{2+} ion. Accordingly, [Ba^{2+}] is expressed by eq 2, where the product AR × [R—COO^-] represents the concentration of R—COO^- groups accessible to Ba^{2+} at a given solution pH. Equation 2 suggests that the concentration of Ba^{2+} that associates with the *accessible* R—COO^- groups at a certain solution pH may be predicted based on the total concentration of R—COO^- groups, and the NN and AR parameters at the same pH. The following sections address the experimental determination of NN and AR.

$$[Ba^{2+}] = \frac{AR \times [R{-}COO^-]}{NN} \qquad (2)$$

Experimental Determination of the Neutralization Number (NN) for Ba^{2+}. The dependence of NN (i.e., the average number of R—COO^- groups neutralized per Ba^{2+} ion) on the concentration of sites neutralized by Ba^{2+} was studied by performing Ag^+-Ba^{2+} ion-exchange experiments at various solution pH conditions (see Table 1 and Figure 3). The concentrations of Ag^+ in the active layer before (column 2) and after (column 3) exchange, and the concentration of Ba^{2+} in the active layer after exchange (column 4) were determined by RBS. The calculated drop in Ag^+ concentration

TABLE 1. Experimental Results for Ag^+-Ba^{2+} Ion-Exchange Experiments and Corresponding Values for Neutralization Number (NN), Coefficient *a*, and Accessibility Ratio (AR) in the Polyamide Active Layer of the FT30 RO Membrane

column 1	column 2	column 3	column 4	column 5 = column 2-column 3	column 6 = column 5/column 4	column 7 = 2 × column 4 − column 5	column 8[d]	column 9	column 10
exp. (pH_1[a])	Ag^+ before IX[b] [M]	Ag^+ after IX[b] [M]	Ba^{2+} after IX[b] [M]	Ag^+ displaced by Ba^{2+} [M]	NN [−]	*a*[c] [M]	AR [−][d]	pH_2[e]	Location in SWE[f]
1 (9.51)	0.271	0.163	0.071	0.108	1.511	0.035	0.40	9.53	FT30-L2
2 (9.48)	0.239	0.102	0.085	0.137	1.614	0.033	0.40	9.53	FT30-L3
3 (7.58)	0.115	0.058	0.046	0.057	1.236	0.035	0.39	7.20	FT30-L4
4 (7.50)	0.121	0.058	0.049	0.063	1.282	0.035	0.39	7.20	FT30-L5
5 (10.26)	0. 409	0.270	0.087	0.139	1.598	0.035	0.40	10.30	FT30-L5
1−5[g] (7.50−10.26)	–	–	–	–	–	0.035	0.40	4.92−10.30	FT30-L2-FT30-L5

[a] pH_1 = pH of the ion-exchange experiment. [b] IX = ion exchange. [c] *a* equals the *x* and *y* values at the intercept between the lines of slope one and two in Figure 3a, also equivalent to the concentration of sites neutralized by Ba^{2+}, i.e., coordinate in Figure 3b, at which NN departs from unity. [d] Calculated using eqs 2 and 3, column 7, and the [R−COO^-] and [Ba^{2+}] information in Figure 2a at the pH indicated in column 9. [e] pH_2 = pH of the Ba^{2+}-probing experiment from which the [Ba^{2+}] value used to calculate AR in column 8 was obtained. [f] SWE = Spiral-wound element; column 10 indicates different locations within the SWE from which the membrane samples used in the corresponding ion-exchange experiment were taken (see also Materials and Methods section). [g] Coefficient *a* obtained through the linear fit of the data from experiments 1−5 in Figure 3a. AR was calculated as the average of the AR values obtained for each of the pH conditions at which [Ba^{2+}] was measured in Figure 2a (see Figure 4), except for pH 3.42 at which AR = 1 (see Figure 2b and corresponding discussion).

in the active layer (column 5) corresponds to the concentration of Ag^+ displaced by Ba^{2+}, and therefore to the concentration of R−COO^- sites neutralized by Ba^{2+} (*y*-axis in Figure 3a). The concentration of Ba^{2+} neutralizing those sites (*x*-axis in Figure 3a) is given by the Ba^{2+} concentration after exchange (column 4).

Figure 3a shows that all experimental points obtained through the ion-exchange experiments lie on a straight (blue dashed-dotted) line with a slope of ≈2 (best fit $y = 2.032x - 0.037$). The slope of two indicates that as the degree of ionization of R−COO^- groups increases in the concentration range of ionized sites at which the experiments were performed, every two additional sites that ionize are neutralized by one Ba^{2+} ion (slope = $\Delta y/\Delta x \approx 2/1 \approx 2$). The (*x*, *y*) coordinates of each of the experimental points in Figure 3a were used to obtain the corresponding neutralization numbers ($NN = y/x$) which are presented as symbols in Figure 3b; the experimental NN values lie between one and two, the theoretical lower and upper limits, respectively, of NN.

Even though we were not able to obtain ion-exchange data at lower concentrations in Figure 3 due to the inability of our sample analysis procedure to accurately differentiate the Ag^+ and Ba^{2+} signals at these lower concentrations, the occurrence of a one-to-one stoichiometry (NN = 1) at the lower concentration limit in Figure 3 is confirmed by the ion-probing results in Figure 2 showing that [R−COO^-] and [Ba^{2+}] are approximately equal (≈0.01 M) at pH 3.42. Accordingly, as the degree of ionization increases at these relatively low concentrations of R−COO^- groups in Figure 3a, every two additional sites that ionize are neutralized by two Ba^{2+} ions resulting in a (blue) dashed line with slope of one (slope = $\Delta y/\Delta x \approx 2/2 \approx 1$). The corresponding $NN = y/x = 1$ representing the one-to-one stoichiometry of association between accessible R−COO^- groups and Ba^{2+} ions is depicted by the (blue) dashed line in Figure 3b.

Equation 2 and the equations of the two limiting linear behaviors depicted in Figure 3a for the stoichiometry of association between additional accessible carboxylic groups that ionize and the Ba^{2+} ions that neutralize them, i.e., $\Delta y/\Delta x = 1 \rightarrow y = x$ and $\Delta y/\Delta x = 2 \rightarrow y = 2x - a$, were used to obtain eq 3 describing the behavior of $NN = y/x$ as a function of the concentration of sites neutralized by Ba^{2+} ion (AR × [R−COO^-]). The parameter *a* in eq 3 represents the concentration of accessible R−COO^- groups at which the stoichiometry of association between the additional sites that ionize and the Ba^{2+} ions that neutralize them (i.e., $\Delta y/\Delta x$) changes from one-to-one to two-to-one (see point A in Figure 3a); *a* is also equal to the maximum concentration of accessible ionized sites at which NN = 1 (see Figure 3b). The parameter *a* is a set value for the specific membrane-counterion system studied and does not depend on pH. We note that the magnitude of $a = 0.035$ M for the FT30 membrane-Ba^{2+} system is higher than 0.01 M at which the ion-probing data shows that a one-to-one stoichiometry still occurs. Equation 3 is valid when AR × [R−COO^-] > *a*, otherwise NN = 1.

$$NN = 2 \times \left(\frac{AR \times [R - COO^-]}{AR \times [R - COO^-] + a} \right) \quad (3)$$

Column 2 in Table 1 reveals the occurrence of variability in the concentration of R−COO^- groups at different locations of the spiral-wound element. R−COO^- concentrations for locations FT30-L2 through FT30-L5 were 60−110% of those in location FT30-L1 at the corresponding solution pH (see Figure 2a). It is important to notice, however, that the variability in the concentration of R−COO^- groups for different locations in the spiral-wound element at a given pH does not antagonize the purpose of Figure 3. The purpose of Figure 3 is *not* to provide ion-exchange capacity information, but information on the stoichiometry of the association between neutralized R−COO^- groups and Ba^{2+} ions as a function of the concentration of the former regardless of the pH at which any given concentration occurs.

Experimental Determination of the Accessibility Ratio (AR) for Ba^{2+}. From the analysis above of Figure 2, we

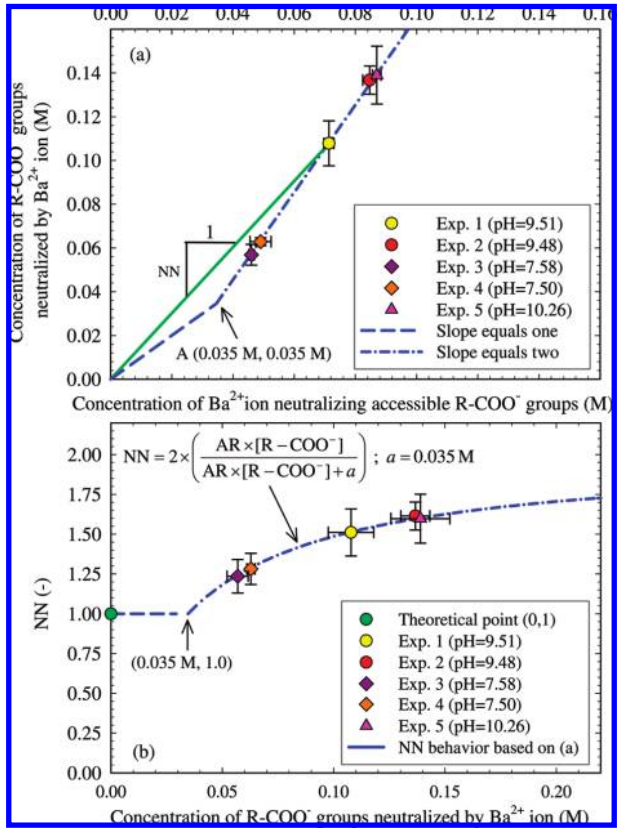

FIGURE 3. Stoichiometry of the association between R—COO⁻ groups neutralized by Ba^{2+} ion in the polyamide active layer of the FT30 RO membrane and the Ba^{2+} ions neutralizing them. (a) Limiting one-to-one (blue dashed line) and two-to-one (blue dashed-dotted line) correspondence between accessible R—COO⁻ groups and Ba^{2+} ion. The symbols are the experimental ion-exchange data presented in Table 1. The neutralization number (NN) for any given point is calculated as the corresponding *y/x* ratio as illustrated by the continuous (green) line for Experiment 1. (b) Behavior of the neutralization number for Ba^{2+} ion (NN) as a function of the concentration of R—COO⁻ sites that it neutralizes. Symbols are the NN values of the five experimental sets from (a)-see also Table 1. The (blue) dashed and dashed-dotted lines are the NN values of the points that belong to the (blue) dashed and dashed-dotted lines in (a). Error bars indicate standard error.

concluded that ≈100% of the carboxylic groups ionized at pH 3.42 were accessible to Ba^{2+} ion (AR = 1), and that this was not the case at the other pH conditions investigated. For the experimental pH values of 4.92 and above, we calculated the corresponding AR values using eqs 2 and 3 with $a = 0.035$ M, and the corresponding experimental [Ba^{2+}] and [R—COO⁻] values at each pH from Figure 2a. The results, shown in Figure 4, reveal that the accessibility ratio is approximately constant at AR = 0.40 in the pH range 4.92−10.30, indicating that only ≈40% of the ionizable carboxylic groups in the active layer of FT30 membrane are accessible to Ba^{2+}. The inaccessible R—COO⁻ groups would therefore be located in regions of the active layer accessible only through pores smaller than Ba^{2+} ion, or of such a size and geometry that a "two-way traffic" of incoming Ba^{2+} ions and out coming protons (H^+) is not possible as it has been proposed to occur in other ion-exchange systems (*24*).

The existence of a pore size distribution in the active layer of FT30 membrane (*8*) is one of the factors that possibly determines the broad pH range of ionization of its R—COO⁻ groups (*14, 25*) as a result of the decreasing dielectric constant of water with decreasing size of the nanopores where it is confined (*4, 26, 27*), and the

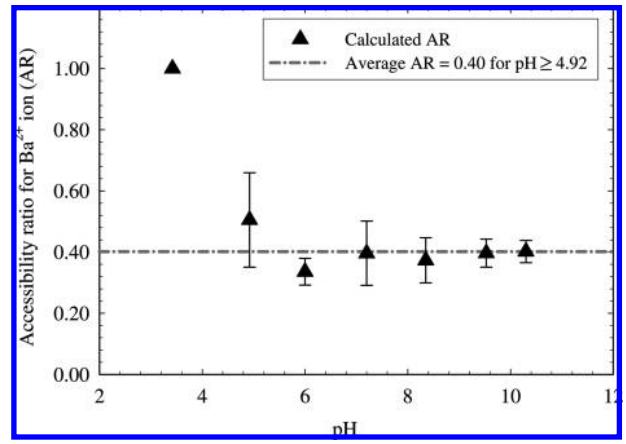

FIGURE 4. Accessibility ratio for Ba^{2+} ion (AR) in the polyamide active layer of the FT30 RO membrane. Symbols are the values obtained by solving eqs 2 and 3 simultaneously using the [R—COO⁻] and [Ba^{2+}] information in Figure 2a, and $a = 0.035$ M from Figure 3b, where *a* is the concentration of sites neutralized by Ba^{2+} at which the neutralization number (NN) for Ba^{2+} departs from unity. AR was calculated for the pH values at which [Ba^{2+}] was determined experimentally (see Figure 2a), except pH 3.42 at which AR = 1 (see Figure 2b and corresponding discussion). Error bars indicate standard error. The dashed-dotted line is the average AR = 0.40 value in the pH range 4.92−10.30.

increasing pK_a value of carboxylic groups with decreasing dielectric constant of the surrounding medium (*28*). Accordingly, the broad pH range of ionization of R—COO⁻ groups (see Figure 2a) suggests that R—COO⁻ groups are distributed in pores of different sizes. The constant accessibility ratio AR = 0.40 for the relatively broad experimental pH range of 4.92−10.30 therefore suggests that there is interconnectivity between pores of different sizes in the active layer. Even if carboxylic groups with different pK_a values are likely located in pores of different sizes, the interconnectivity between pores makes all ionized sites approximately equally accessible (or inaccessible) to Ba^{2+}. Additionally, even if carboxylic groups are located in the larger pores ($r_{\text{Larger Pore}} = 3.5-4.1$ Å (*8*)) which are bigger than Ba^{2+} ($r_{Ba^{2+}} = 1.49-1.75$ Å (*17*)), the pore may be accessible only through the smaller pores due to pore interconnectivity, which would make the functional groups located in the larger pore effectively inaccessible to Ba^{2+} (see location (e) in Figure 1).

We used eqs 2 and 3 to calculate the concentration of Ba^{2+} associated with R—COO⁻ groups as a function of pH using as input the experimentally determined parameter $a = 0.035$ M, the constant accessibility ratio AR = 0.40, and the total concentration of R—COO⁻ groups at each corresponding pH. The results, shown as a (blue) dashed-dotted line in Figure 2a, are in close agreement with the experimental data. We point out that the two constant parameters $a = 0.035$ M and AR = 0.40 describe the difference between [Ba^{2+}] and [R—COO⁻] *as a function of pH* without recourse to any other parameters (e.g., a change in acid dissociation constants). Accordingly, the agreement between the calculated [Ba^{2+}] and the experimental data suggests that the difference between [Ba^{2+}] and [R—COO⁻] is indeed primarily the result of steric and charge effects on Ba^{2+} ion.

Prediction of [Ba^{2+}]. We have demonstrated that we can describe the stoichiometry of association between R—COO⁻ groups and Ba^{2+} as two limiting lines with slopes of one ($y = x$) and two ($y = 2x - a$) in a plot of the concentration of ionized sites neutralized by Ba^{2+} as a function of the concentration of Ba^{2+} neutralizing those sites (see Figure 3a). Such realization indicates that it is possible to obtain

a good estimate of the parameter *a* from any ion-exchange experiment whose data point lies on the line of slope of two. Additionally, the demonstrated constant accessibility ratio in the pH range 4.92−10.30 reveals that we can use the estimated *a* value to determine AR (see column 8 in Table 1) by plugging in eqs 2 and 3 [R−COO^-] and [Ba^{2+}] values at any *one* pH condition. Any of the resulting pairs of *a* and AR values (see Table 1) obtained through Ba^{2+}-probing and ion-exchange experiments *at one pH* can then be used with eqs 2 and 3 and the [R−COO^-] data in Figure 2a to *predict* [Ba^{2+}] *as a function of pH*. The results (presented in SI Figure S3) are in very close agreement with the (blue) dashed-dotted line of Figure 2b.

The methods developed in the present study and our previous work (*14*) provide tools for the *quantitative* study of the effects that functional groups in the active layer of RO/NF membranes and their interaction with ionic contaminants have on membrane performance. For example, our procedures can be used to study the effect that the concentration of functional groups in active layers has on water flux and/or ion rejection. Also, using the AR parameter as a metric of the steric effects that ionic contaminants experience in active layers, the effects of steric hindrance on ion rejection can be studied. Such studies will contribute to build a more complete understanding of the mechanisms of contaminant transport through active layers and guide the development of improved RO/NF membranes.

Acknowledgments

RBS analyses were carried out in the Center for Microanalysis of Materials, University of Illinois, partially supported by the U.S. Department of Energy under grant DEFG02-91-ER45439. We acknowledge Doug Jeffers for assistance in RBS analyses, and Tasuma Suzuki for helpful discussion. This work was supported by the National Science Foundation Environmental Engineering and Technology program under agreement number BES-0332217, and the WaterCAMPWS, a Science and Technology Center of Advanced Materials for the Purification of Water with Systems under agreement number CTS-0120978. The opinions in this paper do not necessarily reflect those of the sponsor.

Supporting Information Available

Materials and Methods (extended version); Figure S1 (Effect of the anion of the barium salt on the concentration of Ba^{2+} that associates with R−COO^- groups in the active layer of FT30 RO membrane); Figure S2 (Example of a spectrum obtained from the RBS analysis of an FT30 RO membrane sample probed with Ba^{2+} ion at pH 10.3); and Figure S3 (Comparison between the prediction of [Ba^{2+}] as a function of pH using the six different sets of *a* and AR values shown in Table 1). This material is available free of charge via the Internet at http://pubs.acs.org.

Literature Cited

(1) Petersen, R. J. Composite reverse osmosis and nanofiltration membranes. *J. Membr. Sci.* **1993**, *83*, 81–150.
(2) Tang, C. Y.; Kwon, Y.-N.; Leckie, J. O. Probing the nano- and micro-scales of reverse osmosis membranes-A comprehensive characterization of physiochemical properties of uncoated and coated membranes by XPS, TEM, ATR-FTIR, and streaming potential measurements. *J. Membr. Sci.* **2007**, *287*, 146–156.
(3) Bellona, C.; Drewes, J. E.; Xu, P.; Amy, G. Factors affecting the rejection of organic solutes during NF/RO treatment-a literature review. *Water Res.* **2004**, *38*, 2795–2809.
(4) Szymczyk, A.; Fievet, P. Investigating transport properties of nanofiltration membranes by means of a steric, electric and dielectric exclusion model. *J. Membr. Sci.* **2005**, (252), 77–88.
(5) Childress, A. E.; Elimelech, M. Relating nanofiltration membrane performance to membrane charge (electrokinetic) characteristics. *Environ. Sci. Technol.* **2000**, *34*, 3710–3716.
(6) Bartels, C. R. A surface science investigation of composite membranes. *J. Membr. Sci.* **1989**, *45*, 225–245.
(7) Shimazu, A.; Ikeda, K.; Miyazaki, T.; Ito, Y. Application of positron annihilation technique to reverse osmosis membrane materials. *Radiat. Phys. Chem.* **2000**, *58*, 555–561.
(8) Kim, S. H.; Kwak, S.-Y.; Suzuki, T. Positron annihilation spectroscopic evidence to demonstrate the flux-enhancement mechanism in morphology-controlled thin-film-composite (TFC) membrane. *Environ. Sci. Technol.* **2005**, *39*, 1764–1770.
(9) Boussu, K.; De Baerdemaeker, J.; Dauwe, C.; Weber, M.; Lynn, K. G.; Depla, D.; Aldea, S.; Vankelecom, I. F. J.; Vandecasteele, C.; Van der Bruggen, B. Physico-chemical characterization of nanofiltration membranes. *Chem. Phys. Chem.* **2007**, *8*, 370–379.
(10) Ben-David, A.; Bason, S.; Jopp, J.; Oren, Y.; Freger, V. Partitioning of organic solutes between water and polyamide layer of RO and NF membranes: Correlation to rejection. *J. Membr. Sci.* **2006**, *281*, 480–490.
(11) Mi, B.; Coronell, O.; Mariñas, B. J.; Watanabe, F.; Cahill, D. G.; Petrov, I. Physico-chemical characterization of NF/RO membrane active layers by Rutherford backscattering spectrometry. *J. Membr. Sci.* **2006**, *282*, 71–81.
(12) Mi, B.; Mariñas, B. J.; Cahill, D. G. RBS characterization of arsenic (III) partitioning from aqueous phase into the active layers of thin-film composite NF/RO membranes. *Environ. Sci. Technol.* **2007**, *41*, 3290–3295.
(13) Zhang, X.; Cahill, D. G.; Coronell, O.; Mariñas, B. J. Partitioning of salt ions in FT30 reverse osmosis membranes. *Appl. Phys. Lett.* **2007**, *91*, 181904.
(14) Coronell, O.; Mariñas, B. J.; Zhang, X.; Cahill, D. G. Quantification of functional groups and modeling of their ionization behavior in the active layer of FT30 reverse osmosis membrane. *Environ. Sci. Technol.* **2008**, *42*, 5260–5266.
(15) Freger, V. Nanoscale heterogeneity of polyamide membranes formed by interfacial polymerization. *Langmuir* **2003**, *19*, 4791–4797.
(16) Afonso, M. D.; Hagmeyer, G.; Gimbel, R. Streaming potential measurements to assess the variation of nanofiltration membranes surface charge with the concentration of salt solutions. *Sep. Purif. Technol.* **2001**, *22−23*, 529–541.
(17) Shannon, R. D. Revised effective ionic radii and systematic studies of interatomic distances in halides and chalcogenides. *Acta Crystallogr.* **1976**, *A32*, 751–767.
(18) Mayer, M.; Duggan, J. L.; Morgan, I. L. In SIMNRA, a simulation program for the analysis of NRA, RBS and ERDA. *Proceedings of the 15th International Conference on the Application of Accelerators in Research and Industry, Denton, TX, 1998*, Denton, TX, 1998; p 541.
(19) IUPAC *Stability Constants Database*; Academic Software: Yorks, UK, 2001.
(20) Chu, W.-K.; Mayer, J. W.; Nicolet, M. A., *Backscattering Spectrometry*; Academic Press: New York, NY, 1978.
(21) Mi, B.; Cahill, D. G.; Mariñas, B. J. Physico-chemical integrity of nanofiltration/reverse osmosis membranes during characterization by Rutherford backscattering spectrometry. *J. Membr. Sci.* **2007**, *291*, 77–85.
(22) Zhang, X.; Cahill, D. G.; Coronell, O.; Mariñas, B. J. Absorption of water in the active layer of reverse osmosis membranes. *J. Membr. Sci.* **2009**, *331*, 143–151.
(23) Albert, A.; Serjeant, E. P. *The Determination of Ionization Constants*, 3rd ed.; Chapman and Hall: London, Great Britain, 1984.
(24) Helfferich, F., *Ion exchange*; McGraw-Hill: New York, 1962.
(25) Wamser, C. C.; Gilbert, M. I. Detection of surface functional group asymmetry in interfacially-polymerized films by contact angle titrations. *Langmuir* **1992**, *8*, 1608–1614.
(26) Senapati, S.; Chandra, A. Dielectric constant of water confined in a nanocavity. *J. Phys. Chem. B* **2001**, *105*, 5106–5109.
(27) Szymczyk, A.; Sbaï, M.; Fievet, P.; Vidonne, A. Transport properties and electrokinetic characterization of an amphoteric nanofilter. *Langmuir* **2006**, *22*, 3910–3919.
(28) Bacarella, A. L.; Grunwald, E.; Marshall, H. P.; Lee Purlee, E. The potentiometric measurements of acid dissociation constants and pH in the system methanol-water. pK_a values for carboxylic acids and anilinium ions. *J. Org. Chem.* **1955**, *20*, 747–762.

ES803595F